Electronic Supplementary Material (ESI) for Environmental Science: Processes & Impacts.
This journal is © The Royal Society of Chemistry 2021

Supplementary Information for

Environmental Science: Processes and Impacts

Adsorption of double-stranded ribonucleic acids (dsRNA) to iron (oxyhydr)oxide surfaces: comparative analysis of model dsRNA molecules and deoxyribonucleic acids (DNA)

Katharina Sodnikar[†], Kimberly M. Parker[‖], Simona R. Stump[†], Laurel K. ThomasArrigo[†] and Michael Sander[†*]

[†]Institute of Biogeochemistry and Pollutant Dynamics, ETH Zurich, 8092 Zurich, Switzerland

[‖]Department of Energy, Environmental & Chemical Engineering, Washington University in St. Louis, St. Louis, Missouri 63130, United States

*To whom correspondence should be addressed.
Michael Sander
Swiss Federal Institute of Technology (ETH) Zurich
DUSYS, IBP
Universitätsstrasse 16, CHN H50.3
8092 Zurich
Switzerland

E-mail: michael.sander@env.ethz.ch
Phone: +41-(0)44 632 8314

Number of pages: 18
Number of figures: 10
Number of tables: 3

S1. Chemicals

Bis(2-hydroxyethyl)aminotris(hydroxymethyl)methane (BisTris, (≥98 %)) was purchased from Sigma-Aldrich (USA), acetic acid glacial (99.8 %) and sodium chloride (99.5 %) were obtained from Fisher Scientific (UK). Sodium acetate trihydrate (≤99 %), sodium carbonate (Na_2CO_3, pro analysis (p.a.)), sodium hydrogen carbonate ($NaHCO_3$, p.a.), magnesium chloride hexahydrate ($MgCl_2*6H_2O$, >99.0%) and sodium dihydrogen phosphate (NaH_2PO_4, ≤99 %) were from Merck (Germany). 2-(Cyclohexylamino)ethanesulfonic acid (CHES, ≥99.5 %) and 4-(2-Hydroxyethyl)piperazine-1-ethanesulfonic acid (HEPES, >99.5 %) were obtained from Fluka Chemie (Switzerland). Hydrochloride acid 37% was obtained from VWR and sodium hydroxide (98.3 %) from Fisher Scientific (UK). QuBit dsDNA broad range (BR) assay kit was purchased at Invitrogen.

S2. Size distribution of nucleic acids (NAs)

The sizes of the NAs (i.e., gDNA, sDNA and polyAU) were analyzed using an Agilent 2200 Tapestation with a genomic DNA ScreenTape (Agilent Technologies) according to the manufacturer's protocol (**Figure S1**). We note that since no ScreenTape was available to detect dsRNA, we used the genomic DNA ScreenTape also for dsRNA detection. While the signal for the model dsRNA (polyAU) was weak (**Figure S1c**), it was sufficiently strong to estimate its size distribution. We additionally determined the NA size distributions by agarose gel electrophoresis (1% agarose in Tris-acetate-EDTA buffer, 100 volts for 30 min, GelRed = fluorescent nucleic acid stain) (**Figure S2**). The results of the Tapestation and the agarose gel electrophoresis analyses were in good agreement (**Figures S1** and **S2**, respectively).

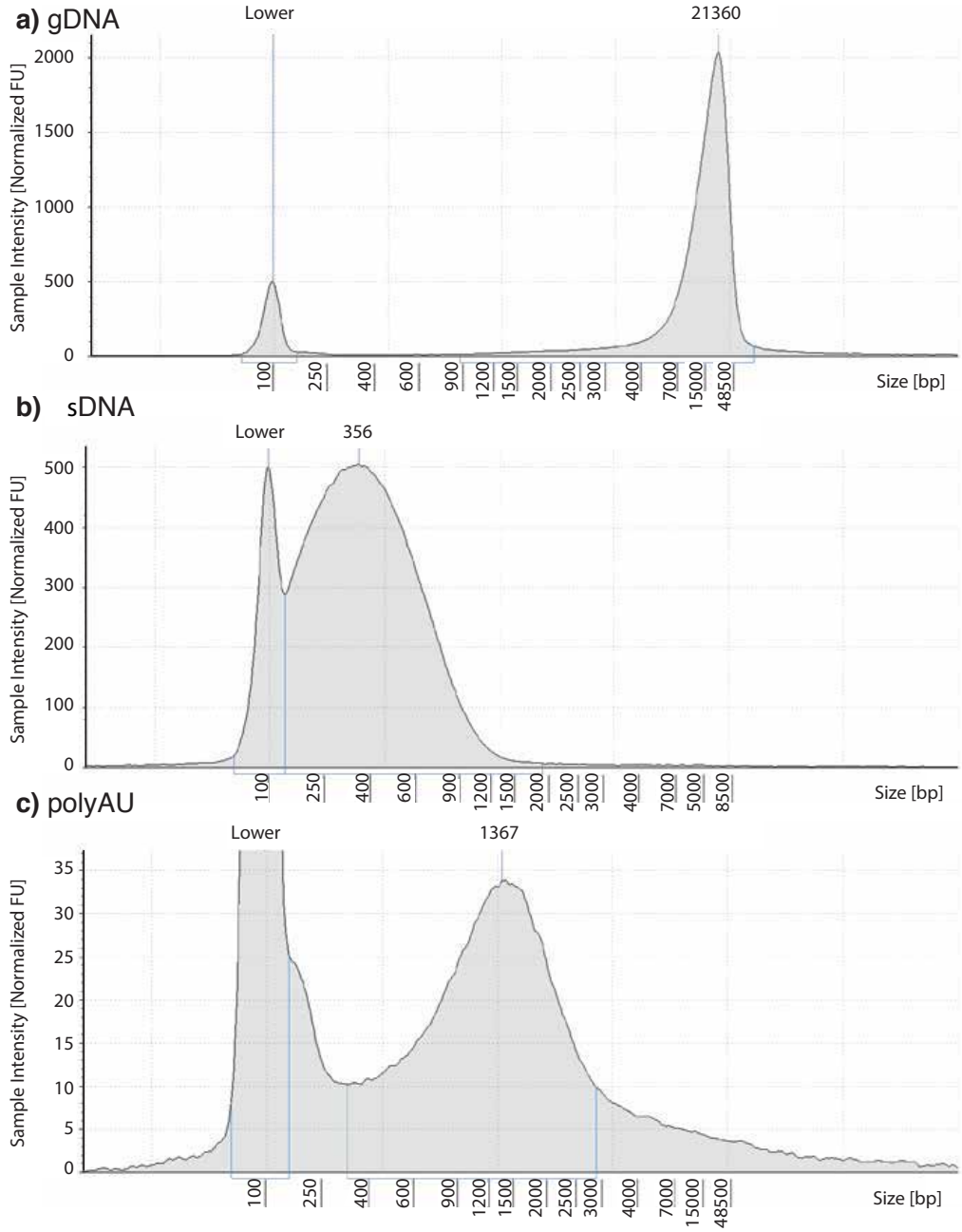

Figure S1. Size distribution of **(a)** genomic DNA (gDNA), **(b)** sheared DNA (sDNA) and **(c)** model dsRNA (polyAU) using a digital electrophoresis (gDNA ScreenTape in the 2200 Agilent Tapestation).

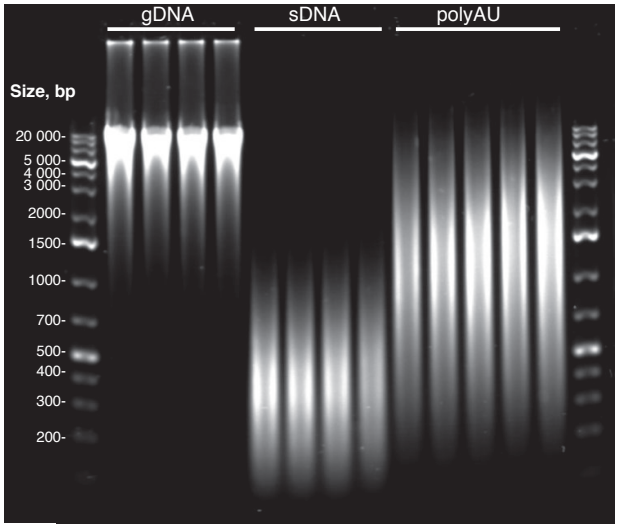

Figure S2. Size distribution of genomic DNA (gDNA), sheared DNA (sDNA) and model dsRNA (polyAU) determined by agarose gel electrophoresis.

S3. Assessment of DNA stability in solution

In a first set of experiments, we assessed the effect of solution chemistry on the stability of gDNA and sDNA in solution. To this end, we prepared DNA solutions of varying DNA concentrations from 2 – 100 µg NA mL^{-1} both in MQ water (resistivity > 18 MΩcm) and in pH 7 buffer (i.e., MQ water containing 3 mM BisTris and 10 mM NaCl as background electrolyte). We subsequently quantified the solution DNA concentration using two different methods: by spectrophotometry with ultraviolet (UV) light absorption at a wavelength of 260 nm (NanoDrop 1000, Witec AG, Switzerland) and by fluorescence reading using a staining protocol (QuBit dsDNA BR Assay kit, fluorescent dye: PicoGreen) measured on a multimode fluorescence microplate reader (Spark, Tecan).

Both DNA quantification approaches resulted in very similar dissolved DNA concentrations for the DNA dilution series prepared in buffered solutions. Furthermore, these concentrations were in good agreement with the DNA concentrations that we expected based on the nominal concentration of the DNA stock (**Figure S3 a and b**). By contrast, the two DNA quantification approaches yielded very different DNA concentrations for the DNA dilution series prepared in MQ water: the DNA concentrations determined spectrophotometrically were higher and, in addition, above the expected DNA concentrations based on the nominal concentration of the DNA stocks (**Figure S3 c and d**). Conversely, the DNA concentrations quantified by fluorescent staining were lower than the expected DNA concentrations. Because the fluorescent dye only stains double stranded DNA[1] and because DNA denaturing results in a higher absorption coefficient,[2] our findings strongly suggest that

(part of) the DNA denatured upon being dissolved in MQ water. DNA denaturation can be rationalized by strong intramolecular electrostatic repulsion between negatively-charged phosphodiester groups in the backbone of the DNA. This repulsion is alleviated when DNA is dissolved in buffered solutions containing ions. A similar finding was reported by Nakayama and coworkers.[3] Based on these results, we subsequently prepared all DNA and dsRNA solutions in buffer containing background electrolytes.

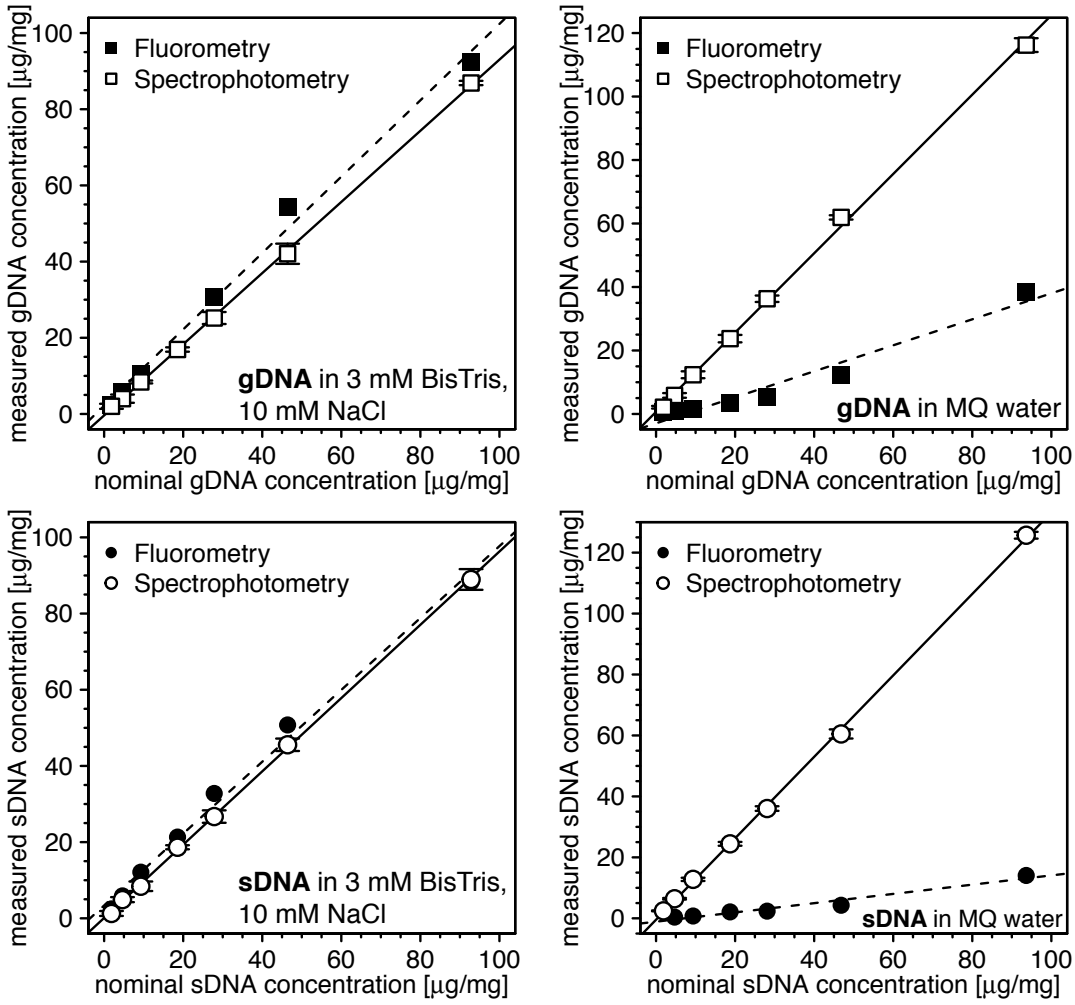

Figure S3. Comparison of measured DNA concentrations determined by spectrophotometric (NanoDrop 1000) and fluorometric (QuBit dsDNA BR genomic DNA kit) DNA quantification relative to the expected nominal DNA solution concentration. Genomic DNA (gDNA) **(a)** and sheared genomic DNA (sDNA) **(b)** diluted in pH 7 buffer (3 mM BisTris, 10 mM NaCl as background electrolyte). gDNA **(c)** and sDNA **(d)** diluted in MQ water. For spectrophotometric measurements: data points and error bars represent the mean and the standard deviation of triplicate determinations. We chose one of the triplicates at each nominal nucleic acid concentration and fluorometrically measured the DNA concentration using the Qubit (single measurement).

S4. Characterization of iron oxides

Mineralogy. We determined the mineralogy of the three iron oxides by X-ray diffraction (XRD). To this end, powdered samples were prepared in plastic sample holders for XRD measurements. The X-ray diffractograms of goethite, lepidocrocite, and hematite were recorded with a D8 Advanced instrument (Bruker) in Bragg-Brentano geometry using Cu Kα radiation (λ = 1.5418 Å, 40 kV and 40 mA) and a high-resolution energy-dispersive 1D detector (LYNXEYE). Diffraction patterns were recorded from 10 to 70°2θ (step size 0.02°2θ and 10 s acquisition time per step). We determined the relative contributions of mineral phases in diffraction patterns by Rietveld quantitative phase analysis (QPA) with published structure files for goethite (ICSD 239321),[4] hematite (AMCSD 0000143),[5] and lepidocrocite (ICSD 93948)[6]. All calculations were performed in TOPAS software (Version 5, Bruker AXS). Only the crystalline phases, which could be identified by the presence of a characteristic diffraction peaks, were accepted for the final fits (i.e., no amorphous phases/ferrihydrite were fitted as it has been shown that contents of such phases could only be quantified with very large uncertainties in samples in which such phases are present at only low concentration (as was the case here)).[7] The Goodness of Fit (GOF) is defined as R_{wp}/R_{exp} (with R_{wp} and R_{exp} being the weighted profile and the expected R-factor, respectively).

Table S1. Mineral contributions determined by Rietveld Quantitative Phase Analyses of XRD patterns for the iron oxides used in this study.

Iron oxide	Commercial product name	R_{wp}[a]	GOF[b]	Goe (fitted weight-%)	Lep (fitted weight-%)	Hem (fitted weight-%)
Goethite	Bayferrox 910	7.22	2.13	100	0	0
Lepidocrocite	Bayferrox 943	6.67	2.1	2	98	0
Hematite	Bayferrox 105 M	7.80	2.26	0	0	100

[a]Weighted profile R-factor. [b]Goodness of Fit (GOF) is defined as R_{wp}/R_{exp}. Goe, Lep, and Hem are abbreviations for goethite, lepidocrocite, and hematite, respectively.

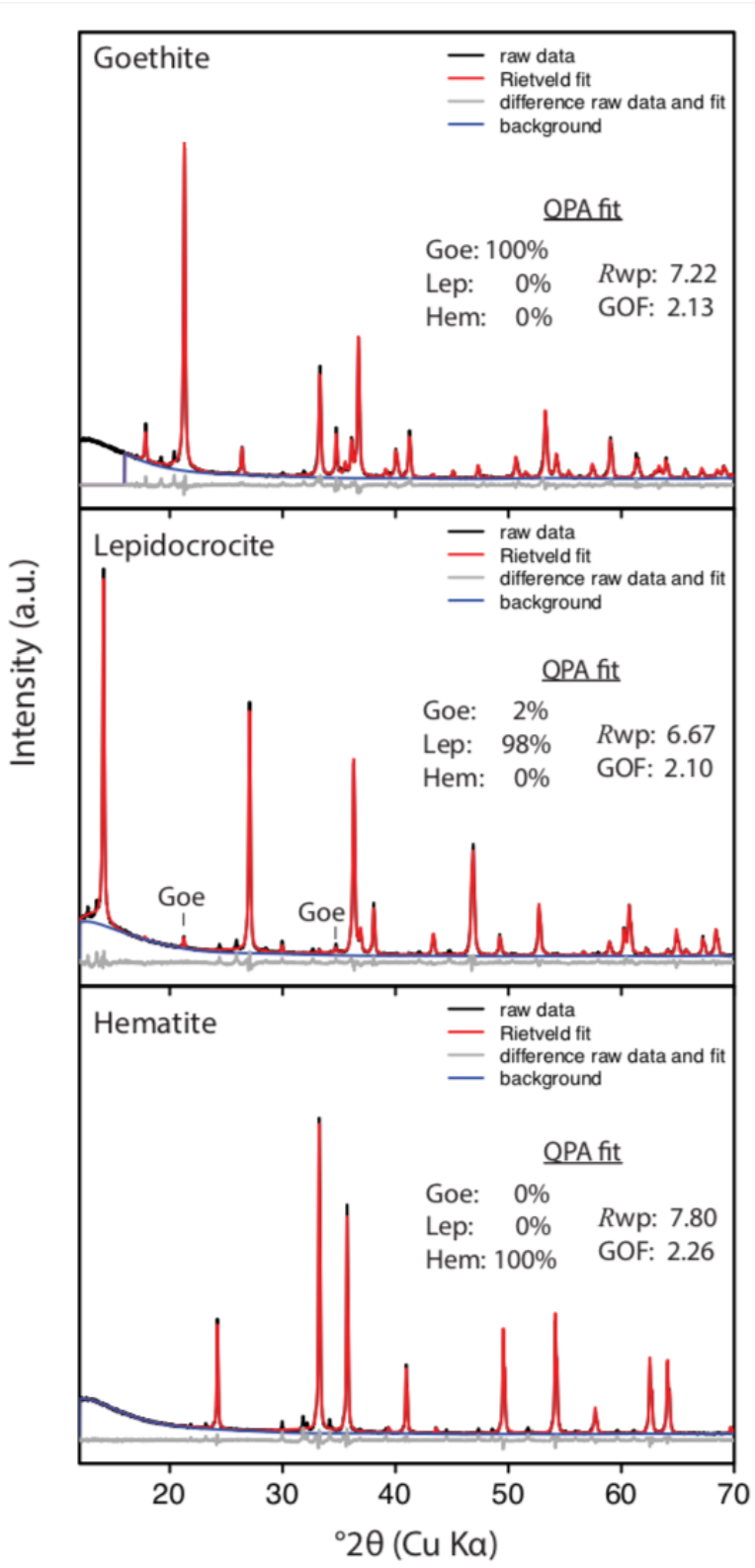

Figure S4. Rietveld Quantitative Phase Analysis (QPA) of the X-ray diffractogram of goethite (Goe), lepidocrocite (Lep), and hematite (Hem). Measured raw data (black), Rietveld fit (red), difference between the two (grey) and background (blue) are shown. Abbreviations: *R*wp = Weighted profile R-factor. GOF = Goodness of Fit is defined as R_{wp}/R_{exp}.

Particle morphology. Dry powders (20 mg) were diluted in 100 mL dispersion agent (0.2% FL70) and sonicated for 10 minutes. The suspension was diluted 1:20 and sonicated for 1 minute in the Vial Tweeter (Hielscher). A drop of this suspension was drawn through a holey carbon TEM grid. The particles were imaged using a scanning transmission electron microscope (HD 2700 Cs, Hitachi, Japan) equipped with a secondary electron detector. The microscope was operated at an acceleration voltage of 200 kV. Scanning microscopy images of the iron oxides, goethite, lepidocrocite and hematite are shown in **Figure S5**.

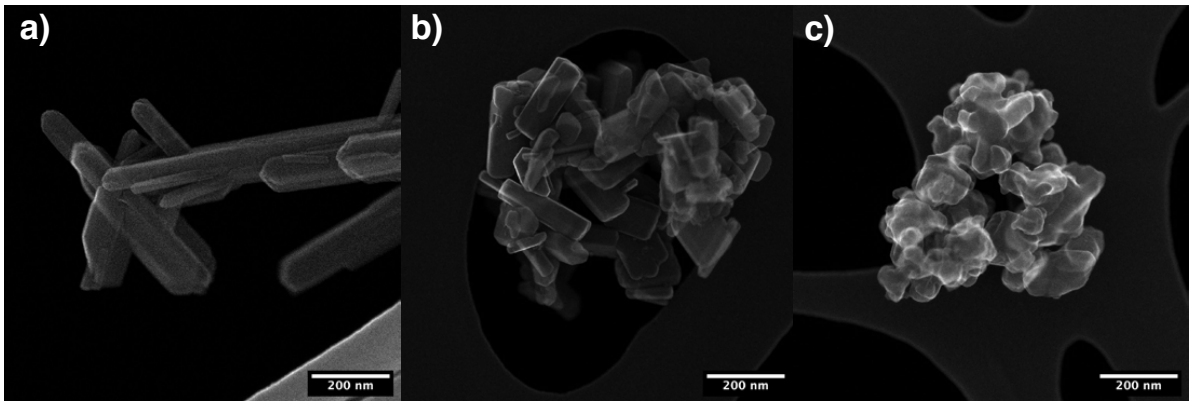

Figure S5. Scanning microscopy images of the iron oxides goethite **(a)** (acicular particles), lepidocrocite **(b)**, and hematite **(c)**.

S5. Surface site speciation of goethite, lepidocrocite and hematite

Speciation diagrams of hydroxyl groups on the surfaces of goethite, lepidocrocite, and hematite are shown in **Figure S6**. These speciation diagrams where calculated based on their published acid dissociation constants[8-10] and according to Equation S1.

$$\left|\equiv Fe-OH_2^+ \overset{pK_{a1}}{\rightleftharpoons} \right|\equiv Fe-OH + H^+ \overset{pK_{a2}}{\rightleftharpoons} \left|\equiv Fe-O^- + 2H^+ \right. \qquad \text{Eq. S1}$$

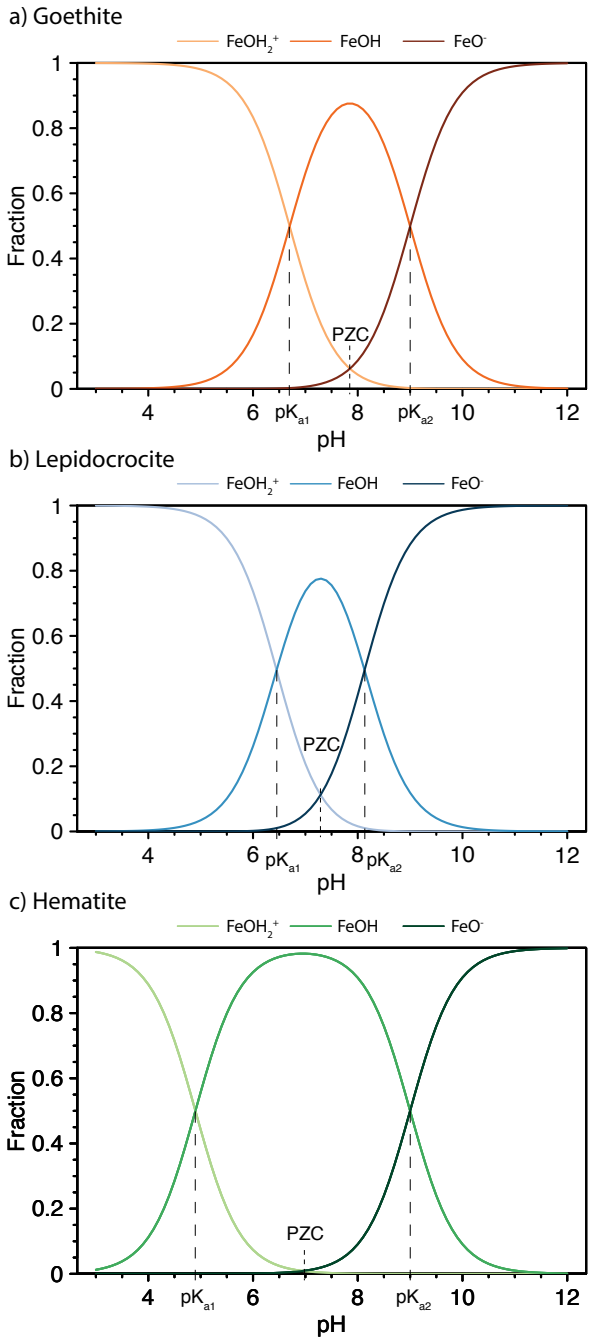

Figure S6. pH dependent speciation of hydroxyl groups on the surface of goethite (**(a)**, pK_{a1} = 6.7, pK_{a2} = 9, both from Müller and Sigg, 1991)[10], lepidocrocite (**(b)**, pK_{a1} = 6.45, pK_{a2} = 8.13, both from Zhang et al., 1992)[8], and hematite (**(c)**, pK_{a1} = 4.9, pK_{a2} = 9, both from Figueroa and MacKay, 2005,[9] used J.T. Baker hematite). PZC= point of zero (net) charge. Fraction refers to the fractional contribution of the respective species to the total pool of the indicated surface sites.

S6. Batch adsorption experiment - method development

To ensure reproducibility in the results of adsorption experiments, we systematically assessed variations in the experimental protocol on the adsorption of gDNA, sDNA, and

polyAU to goethite. The equilibration time for NA adsorption to goethite was 2 hours in these experiments.

First, we tested for potential effects of the order and mode of addition of NA and goethite to the batch reactors on final NA adsorbed concentrations. We varied (i) the order of addition of the NA solution and the goethite suspension (i.e., we added goethite suspension to an NA solution in the batch reactor as well as the NA solution to a goethite suspension in the batch reactor) and (ii) the mode in which the solution and suspension volumes were added (i.e., incremental addition in small volume increments or single addition of the entire volume).

Second, we assessed whether ultrasonication of the goethite suspension had an effect on NA adsorption. We tested (i) sonication prior to addition of the goethite addition (30 minutes at 9 Hz), (ii) sonication prior and during the equilibration time (prior 30 minutes at 9 Hz and during 2 hours at 9 Hz) and, as a control, (iii) no sonication of the goethite suspension at all.

Third, we assessed potential effects of goethite mass loading (i.e., 0.2, 0.5, 2 and 5 mg goethite mL^{-1}) in the batch incubation reactor at constant NA to goethite concentration ratios on NA adsorption. For the subsequent assessment, we compared the adsorbed NA concentrations of triplicate determinations between the different experimental treatments using a one-way ANOVA ($p < 0.05$) and a post hoc Tukey test ($p < 0.05$). The results of these analyses are shown in **Figure S7a-c**.

Order and mode of addition of NA solutions and pre-sonicated GOE suspensions to the batch reactors. The order of addition as well as the mode of addition of sDNA solutions and goethite suspensions to the batch reactors did not significantly affect the adsorbed sDNA concentrations (**Figure S7a**, one-way ANOVA, $p = 0.338$). By comparison, the adsorbed polyAU concentrations were slightly smaller when we added the polyAU in incremental steps (i.e., NA incr.) to the goethite suspension as opposed to all other treatments (one-way ANOVA, $p = 0.002$). The adsorbed gDNA concentration was significantly higher when we added the entire goethite particle suspension in one step as compared to adding it incrementally (Tukey test, $p = 0.024$). For all NAs the adsorbed concentration was slightly lower when we added the NA solution incrementally to the goethite suspension. Based on these findings, we decided to add the goethite suspension dropwise to the NA solution for all subsequent experiments because results were highly reproducible when using this procedure and were only slightly different from the other treatments.

Sonication of the goethite suspensions prior to transfer into batch reactors and/or during adsorptive equilibration. Sonication of the goethite suspension prior to its transfer to

the batch reactors resulted in a significantly higher adsorbed sDNA concentrations compared to the case in which we added non-sonicated goethite suspension (**Figure S7b**, Tukey test, $p = 0.043$). When we sonicated both the goethite suspension prior to the transfer and the batch reactors during the adsorptive equilibration, significantly less polyAU adsorbed to goethite as compared to the other sonication treatments (one-way ANOVA, $p = 0.001$). Conversely, for gDNA the adsorbed concentration was significantly higher when we sonicated prior to the suspension transfer and during the equilibration as compared to reactors run without any sonication (Tukey test, $p = 0.011$). However, overall variations in NA adsorbed amounts between the different sonication treatments were small and not in the same direction for all NAs. Additionally, the sonication during the batch equilibration may have resulted in shearing of some of the NAs (but this was not explicitly tested for). For these reasons, we decided against sonication during batch equilibration but sonicated the goethite suspensions prior to their transfer into the batch reactors in all subsequent experiments.

Changes in the total goethite and NA loadings at a constant loading ratio. Varying the loadings of goethite and NAs had no significant effect on the adsorbed gDNA concentration (**Figure S7c**, one-way ANOVA, $p = 0.061$). However, when we used a goethite concentration of only 0.2 mg mL^{-1}, significantly less sDNA adsorbed compared to the setups in which we used higher goethite concentrations (one-way ANOVA, $p = 9.5 * 10^{-5}$). In the case of polyAU, adsorbed concentrations were significantly smaller when using 0.5 mg goethite mL^{-1} as compared to 5 mg goethite mL^{-1} (Tukey test, $p = 0.029$). At the same time, the standard deviations of calculated adsorbed NA concentrations were larger at the low NA concentration, reflecting analytical uncertainties that resulted from quantifying NA concentrations close to the limit of quantification of the Nanodrop spectrophotometer. Based on these results, we decided to conduct all other experiments at a goethite suspension concentration of 2 mg goethite mL^{-1} because adsorbed concentrations of all NAs were not significantly different between 2 and 5 mg goethite mL^{-1} (Tukey test, $p > 0.05$) and because deviations in the adsorbed NA concentrations between replicate experiments were small in these setups.

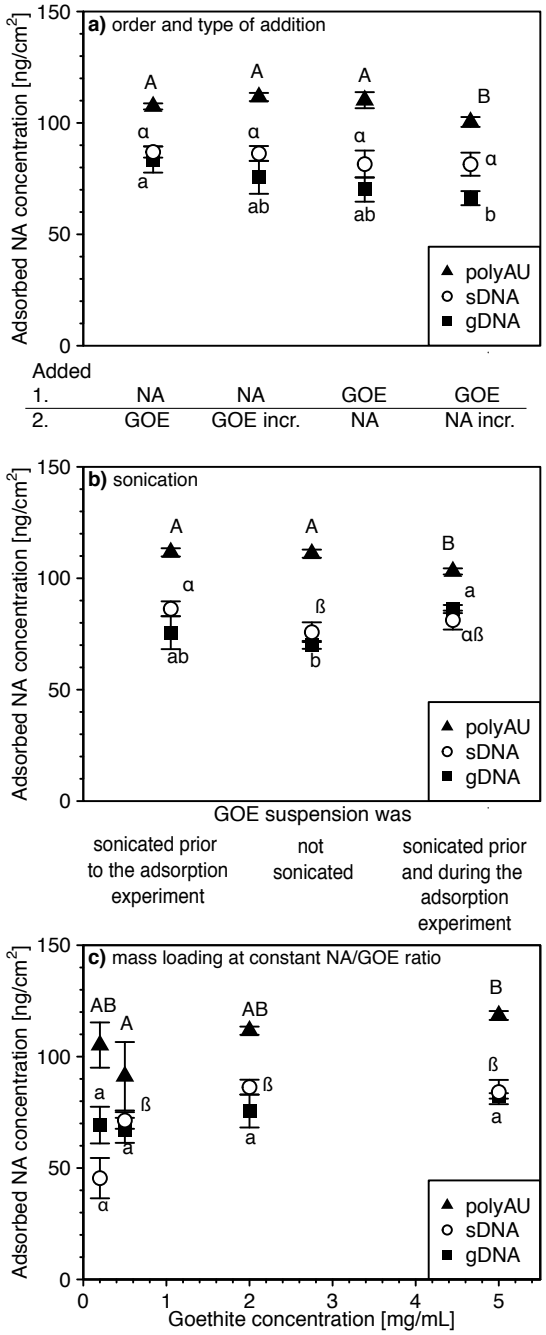

Figure S7. Batch adsorption method validation experiments. **(a)** Effects of order and mode of addition of nucleic acid (NA) and sonicated goethite suspensions (GOE) on the extent of NA adsorption to goethite (incr. refers to incremental addition) ; **(b)** effects of ultrasonication (with and without sonication prior to the experiment, sonication prior and during the experiment) on the adsorbed concentration of NA molecules to goethite; **(c)** adsorbed NA concentrations as a function of the total goethite and NA loadings at a constant loading ratio. The experiments were conducted in pH 7 buffer with 10 mM NaCl as background electrolyte. The equilibration time for NA adsorption was 2 hours. Data points and error bars represent the mean and the standard deviation of triplicate reactors run in parallel. Comparisons between different treatments were performed using a one-way ANOVA ($p < 0.05$) and a post-hoc Tukey ($p < 0.05$). Adsorbed NA concentrations with different letters (i.e., A, B or a, b) are statistically significantly different.

S7. Kinetics of NA adsorption to the iron oxides

Kinetic fit. To determine pseudo-first-order adsorption rate constants and maximum adsorption capacities, we fitted the kinetic adsorption data with the Lagergren's pseudo-first order adsorption model[11] (Equation S2) using a non-linear least squares analysis in Excel (Solver add-in). The Lagergren's pseudo-first order adsorption model[11] is given by the following equation:

$$q_t = q_{max} * (1 - e^{-k*t}) \qquad \text{Eq. S2}$$

where q_t and q_{max} (both in [ng cm^{-2}]) are the adsorbed NA concentration at a given time t and the final NA adsorption capacity, respectively, *k* is the pseudo-first-order adsorption rate constants [h^{-1}], and t the time [h].

Fitted pseudo-first-order adsorption rate constants (*k*) and adsorption capacities (q_{max}) are given in **Table S2**. Both the fitted adsorption rate constants and the fitted adsorption capacities to goethite were higher for the shorter sDNA and polyAU than the much longer gDNA (**Table S2**). gDNA adsorption to three iron oxides was fastest for lepidocrocite, followed by hematite and goethite. Adsorption capacities decreased in the order goethite > lepidocrocite > hematite.

Table S2. Results of pseudo-first-order model fits to NA adsorption kinetics data to iron oxides.

Sorbate	**Sorbent**	***k* (h^{-1}) ± STDEV**	**q_{max} (ng cm^{-2}) ± STDEV**
gDNA	Goethite	5.07±0.38	78.31±0.50
sDNA	Goethite	9.25±0.18	87.83±0.28
polyAU	Goethite	10.91±0.14	103.62±0.21
gDNA	Lepidocrocite	9.47±0.37	45.45±0.20
gDNA	Hematite	8.91±0.61	15.67±0.17

Normalization of the kinetic data by the hydroxyl group density. We replotted the kinetic data from the manuscript (**Figure 1b**) after normalizing the adsorbed gDNA masses to the hydroxyl group surface density (i.e., number of OH groups per nm^2) of the respective iron oxide (**Figure S8**). The published hydroxyl group surface density was 5.5 OH groups

nm^{-2} for goethite (from Müller and Sigg, 1991)[10], 1.67 OH groups nm^{-2} for lepidocrocite (from Zhang et al., 1992)[8], and 0.7 OH groups nm^{-2} for hematite (from Ruf, 1992)[12].

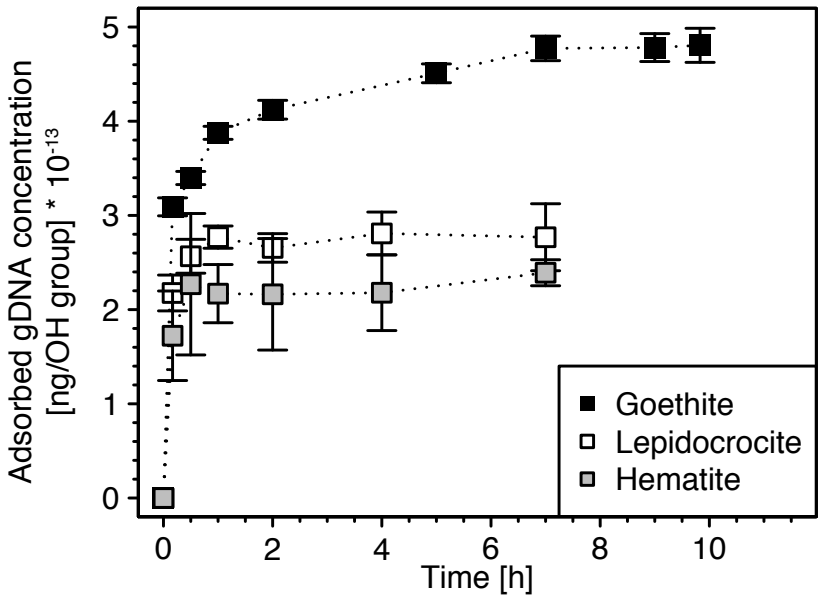

Figure S8. Assessment of gDNA adsorption kinetics to three iron oxides goethite, lepidocrocite and hematite, expressed in adsorbed gDNA masses normalized to the hydroxyl group surface density of the respective iron oxide (goethite: 5.5 OH groups nm^{-2} from Müller and Sigg, 1991[10]; lepidocrocite: 1.67 OH groups nm^{-2} from Zhang e al., 1992[8]; hematite: 0.7 OH groups nm^{-2} from Ruf, 1992[12]). Data points and error bars represent the mean and the standard deviation of triplicate reactors run in parallel. We replotted the data from Figure 1b in the manuscript but normalized adsorbed concentrations to the hydroxyl group surface density of the respective iron oxide.

S8. Langmuir fit of concentration-dependent NA adsorption data

We fitted the concentration-dependent NA adsorption data with the Langmuir isotherm model[13] (equation S3) using a non-linear least squares analysis in Excel (Solver add-in). The Langmuir isotherm model[13] is given by equation S3:

$$q = \frac{q_{max} * K * c(NA)}{1 + K * c(NA)} \qquad \text{Eq. S3}$$

where q and q_{max} (both [ng cm^{-2}]) are the adsorbed NA concentration at equilibrium and the maximum adsorbed NA concentration, respectively, K is the Langmuir equilibrium adsorption coefficient [mL ng^{-1}], and c(NA) is the NA solution concentration at equilibrium [ng mL^{-1}].

We discuss the Langmuir adsorption model fits in the Supporting information only. This approach reflects the fact that the Langmuir isotherm model is derived on the basis of a number of assumptions that are not fulfilled for the adsorption of polyelectrolytes. These assumptions include, but are not limited to, reversible NA adsorption as well as identical footprints (and hence conformations) of the NA molecules in adsorbed states. Despite these considerations, we decided to fit the experimental data to quantitatively describe the concentration-dependent NA adsorption and compare fitted q_{max} values that we determined independent of a model fit, as described in the main text.

Table S3 lists the fitted Langmuir equilibrium adsorption coefficients (K) and the maximum adsorption capacities (q_{max}). Because all added NAs adsorbed to the iron oxide surfaces at low initial solution concentrations, the fitted K values have a relatively large uncertainty. Fitted q_{max} were in good agreement with calculated adsorption capacities (**Figure S9**). This is also true for the fitted q_{max} obtained by applying the Lagergren's pseudo-first order kinetic model[11] to the kinetic data (see section S7 above).

Table S3. Results of fits of the Langmuir adsorption model to the concentration-dependent NA adsorption data.

Sorbate	**Sorbent**	**K [mL ng^{-1}] ± STDEV (*10^{-3})**			**q_{max} [ng cm^{-2}] ± STDEV**		
		pH 5	**pH 7**	**pH 9**	**pH 5**	**pH 7**	**pH 9**
gDNA	Goethite	0.79 ±0.2	1.01 ±0.33	0.77 ±0.28	105.11 ±1.29	82.08 ±5.27	69.40 ±5.11
sDNA	Goethite	190.48 ±66.93	4.5 ±1.26	8 2.48	118.78 ±2.34	82.91 ±1.5	61.13 ±1.03
polyAU	Goethite	122.83 ±41.86	21.21 ±7.08	1.75 ±0.47	156.7 ±3.23	101.04 ±1.66	77.57 ±1.87
gDNA	Lepidocrocite		1.08 ±0.07			57.12 ±0.6	
sDNA	Lepidocrocite		2.39 ±1.28			63.63 ±1.75	
polyAU	Lepidocrocite		0.54 ±0.13			86.58 ±3.22	
gDNA	Hematite		0.25 ±0.03			17.44 ±0.4	
sDNA	Hematite		0.53 ±0.10			15.22 ±0.33	
polyAU	Hematite		0.31 ±0.11			17.44 ±0.76	

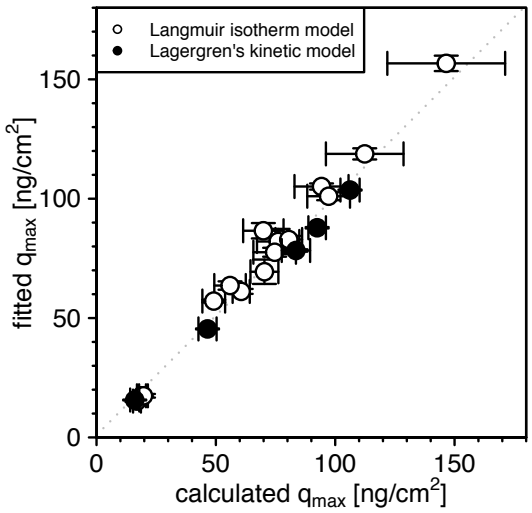

Figure S9. Comparison of model fitted maximum adsorption capacities (fitted q_{max}) and q_{max} values calculated as described in the main text (calculated q_{max}). We fitted the concentration-dependent adsorption data with the Langmuir isotherm model[13] (open circles) and kinetic adsorption data with the Lagergren's pseudo-first order kinetic model[11] (filled circles).

S9. Phosphate concentration dependent adsorption to goethite

We assessed the concentration-dependence of phosphate adsorption to goethite at initial phosphate concentrations of 0.05, 0.1, 0.2, 0.5, and 1 mM. Upon stirring (600 rpm, Variomag Telemodul 20 P, Sterico AG, Switzerland), we dropwise added an aliquot of a sonicated goethite stock suspension to the phosphate solutions in 2 mL tubes (Eppendorf Protein LoBind). The final goethite suspension concentration was 2 mg mL^{-1}. After an equilibration time of 4 hours, we filtered (nominal cutoff 0.25 μm cellulose acetate filters, BGB) the phosphate-goethite suspensions to remove goethite particles, and we determined the non-adsorbed phosphate concentration in the filtrate by ion chromatography (940 Professional IC Vario from Metrohm; column: Metrosep A Supp 5 (250 mm x 4mm), mobile phase: 3.2 mM Na_2CO_3 and 1 mM $NaHCO_3$).

In phosphate adsorption experiments to goethite, phosphate was completely depleted from solution at initial phosphate concentrations below 0.05 mM, demonstrating high affinity of phosphate to goethite surfaces (**Figure S10**). Increasing the initial phosphate concentration

to 0.1 mM resulted in increased phosphate adsorption which, at higher solution concentrations, leveled off at an adsorbed concentration of approximately 2.7 µmol phosphate m^{-2}. This value is in good agreement with reported phosphate adsorption capacities on goethite.[14-19] At this concentration, we expect that phosphate occupied all adsorption sites on the goethite surface.

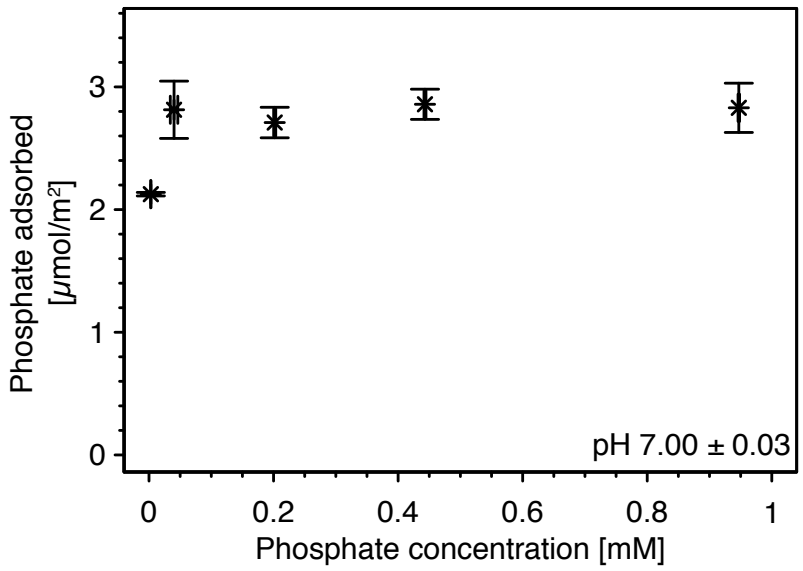

Figure S10. Concentration-dependent phosphate adsorption to goethite determined by solution depletion of phosphate in batch equilibration reactors (at pH 7 ± 0.03, 3 mM BisTris and 10 mM NaCl as background electrolyte). Data points and error bars represent the mean and the standard deviation of the results of triplicate adsorption experiments run in parallel.

References

1 V. L. Singer, L. J. Jones, S. Y. Analytical1997, Characterization of PicoGreen reagent and development of a fluorescence-based solution assay for double-stranded DNA quantitation, *Anal. Biochem.*, 1997, **249**, 228–238.

2 R. R. Alexander and J. M. Griffiths, in *Basic Biochemical Methods*, Wiley, 1993, p. 368.

3 Y. Nakayama, H. Yamaguchi, N. Einaga and M. Esumi, Pitfalls of DNA Quantification Using DNA-Binding Fluorescent Dyes and Suggested Solutions, *PLoS ONE*, 2016, **11**, e0150528.

4 E. Zepeda-Alarcon, A. Gualtieri, G. King, K. Page, S. C. Vogel, H. W. Wang, H. R. Wenk and H. Nakotte, Magnetic and nuclear structure of goethite (α-FeOOH): a neutron diffraction study, *J. Appl. Crystallogr.*, 2014, **47**, 1983–1991.

5 R. L. Blake, R. E. Hessevick, T. Zoltai and L. W. Finger, Refinement of the hematite structure, *Am. Mineral.*, 1966, **51**, 123–129.

6 A. P. Zhukhlistov, Crystal structure of lepidocrocite FeO(OH) from the electron-diffractometry data, *Crystallogr. Rep.*, 2001, **46**, 730–733.
7 L. K. ThomasArrigo, J. M. Byrne, A. Kappler and R. Kretzschmar, Impact of Organic Matter on Iron(II)-Catalyzed Mineral Transformations in Ferrihydrite–Organic Matter Coprecipitates, *Environ. Sci. Technol.*, 2018, **52**, 12316–12326.
8 Y. Zhang, L. Charlet and P. W. Schindler, Adsorption of protons, Fe(II) and Al(III) on lepidocrocite (γ-FeOOH), *Colloids Surf.*, 1992, **63**, 259–268.
9 R. A. Figueroa and A. A. MacKay, Sorption of oxytetracycline to iron oxides and iron oxide-rich soils, *Environ. Sci. Technol.*, 2005, **39**, 6664–6671.
10 B. Müller and L. Sigg, Adsorption of lead(II) on the goethite surface: Voltammetric evaluation of surface complexation parameters, *J. Colloid Interface Sci.*, 1991, **148**, 517–532.
11 S. Lagergren, *Zur Theorie der sogenannten Absorption gelöster Stoffe*, 1898.
12 A. Ruf, PhD Thesis, ETH Zürich, 1992.
13 I. Langmuir, The constitution and fundamental properties of solids and liquids., *J Am Chem Soc*, 1916, **38**, 2221–2295.
14 J. Antelo, M. Avena, S. Fiol, R. López and F. Arce, Effects of pH and ionic strength on the adsorption of phosphate and arsenate at the goethite–water interface, *J. Colloid Interface Sci.*, 2005, **285**, 476–486.
15 O. K. Borggaard, Effect of surface area and mineralogy of iron oxides on their surface charge and anion-adsorption properties, *Clays Clay Miner.*, 1983, **31**, 230–232.
16 J. Kim, W. Li, B. L. Philips and C. P. Grey, Phosphate adsorption on the iron oxyhydroxides goethite (α-FeOOH), akaganeite (β-FeOOH), and lepidocrocite (γ-FeOOH): a ^{31}P NMR Study, *Energy Environ. Sci.*, 2011, **4**, 4298–4305.
17 R. L. Parfitt, R. J. Atkinson and R. S. C. Smart, The Mechanism of Phosphate Fixation by Iron Oxides, *Soil Sci. Soc. Am. J.*, 1975, **39**, 837–841.
18 M. I. Tejedor-Tejedor and M. A. Anderson, The protonation of phosphate on the surface of goethite as studied by CIR-FTIR and electrophoretic mobility, *Langmuir*, 1990, **6**, 602–611.
19 L. Zeng, X. Li and J. Liu, Adsorptive removal of phosphate from aqueous solutions using iron oxide tailings, *Water Res.*, 2004, **38**, 1318–1326.